Spectral Analysis of Multilevel PWM Strategies Using a One-Dimensional Fourier Series

B. P. McGrath (M'99)

[1]School of Electrical and Computer Engineering,
RMIT University, Melbourne, Australia
brendan.mcgrath@rmit.edu.au

H. du T. Mouton (M'00)

[2]Dept. of Electrical and Electronic Engineering,
University of Stellenbosch, South Africa
dtmouton@sun.ac.za

***Abstract* — This paper presents a novel spectral analysis technique for multilevel modulation. Conventionally, such analyses use a Double Fourier series technique, but this approach can become intractable when complex reference waveforms (e.g. multilevel space vector offsets) and regular sampling processes are considered. In contrast, the strategy proposed in this paper separates the multilevel pulse width modulation (PWM) waveform into a spectral image of the reference, and sideband basis functions which are then expanded using a one-dimensional Fourier series. The coefficients of this Fourier series are defined by a one-dimensional Fourier integral that is simpler in form compared to the corresponding double integral associated with the Double Fourier series. This analysis technique naturally incorporates regular sampling, and a discrete formulation is developed that enables complex PWM reference waveforms, including centered space vector offsets, to be solved. Results of this analysis are validated against previously published multilevel inverter Double Fourier series results and matching switched simulations.**

Keywords* — *Multilevel, Pulse Width Modulation, Double Fourier, Spectral Analysis.

I. INTRODUCTION

Techniques to determine the spectral content of waveforms produced by pulse-width-modulated (PWM) inverters are critically important within the field of power electronics, since minimisation of the harmonic distortion produced by an inverter is one of the primary performance criteria for almost all inverter applications [1]. The simplest approach to determine the spectrum of a PWM waveform is to apply a Fast Fourier Transform (FFT) to time-domain converter switched waveforms generated by a power electronic simulator. However this approach is highly error-prone, and requires considerable skill to avoid introducing aliasing artifacts, end-effects (i.e. inappropriate windowing) and spectral leakage [2]. In contrast analytic approaches to quantify PWM spectra [1],[3]-[5] avoid these pit-falls, and can also provide considerable insights into converter operation. These include the identification of optimal harmonic cancellation [6]-[8], the dynamic modelling of voltage balancing phenomena [9]-[11], and converter modelling for closed loop design purposes [12]. However, analytic approaches are typically quite challenging because PWM waveforms are not generally periodic, and hence cannot be solved using conventional one-dimensional Fourier transform techniques [1].

The accepted approach to address the aperiodic nature of PWM is to use a Double Fourier series [1][3][4]. The PWM waveform is then deconstructed as a two-dimensional function of the reference and carrier phase spaces, resulting in a separately periodic function in each dimension. Evaluation of a Double Fourier integral based on these functions gives the coefficients of the Double Fourier series [1]. This technique has been rigorously applied to all major two-level PWM strategies [1]-[5], accommodating a variety of arbitrary reference waveforms (i.e. 3rd harmonic injection, etc.), and all significant regular sampling variants. Double Fourier series formulations of several multilevel PWM strategies also exist [13]-[16], although the process of constructing the two-dimensional Fourier integral is substantially more complex when compared to the two-level case. Hence closed form solutions for multilevel converters have only been obtained so far for naturally sampled conditions with sinusoidal references [14], and multilevel analytic solutions that account for regular sampling effects and complex reference waveforms (e.g. space vector offsets [16]) remain an open problem.

Recently an alternative PWM spectral analysis approach has been presented based on a one-dimensional Fourier series [18]. This new technique recognises that the PWM pulse train can be expanded as the superposition of the original reference, and a pair of phase modulated sawtooth functions which generate the sideband groups in the PWM spectrum. Spectral computation then reduces to solving a one-dimensional Fourier integral, which is considerably easier than solving the two-dimensional Double Fourier series integral. Regular sampling is also readily incorporated into this approach by multiplying the reference by an impulse-train and convolving it with the well-known Zero Order Hold (ZOH) filter response. However to date this approach has only been demonstrated for two-level PWM strategies [18].

This paper now applies this new technique to multilevel PWM. The basis of the approach is to separate a multilevel waveform into a summation of two-level pulse trains, each linked to a particular disposition band and defined by a discontinuous PWM reference waveform. The spectral content of each pulse train is readily determined using the one dimensional Fourier series methodology presented in [18], and superposition of these results defines the overall multilevel spectrum. Results presented include analytic solutions for previously intractable complications, such as

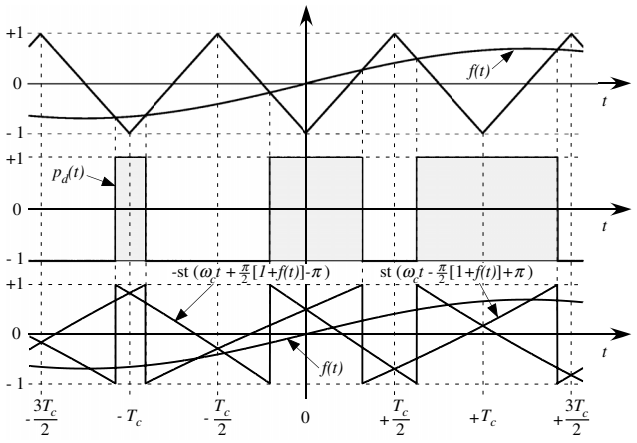

Fig. 1: Construction of a PWM pulse train using superposition.

regular sampled multilevel PWM, and common mode space vector offsets. These results are validated against previously published Double Fourier results and matched simulations.

II. One-Dimensional Spectral Analysis of PWM

Recent work [18] has shown that a double-edge PWM pulse train can be represented as the superposition of three waveforms. This is shown in Fig. 1, where the pulse train $p_d(t)$ is generated from a standard PWM generator that compares a reference waveform $f(t)$ against a triangular carrier with an angular frequency $\omega_c = 2\pi/T_c$. From [18] $p_d(t)$ is equivalent to the superposition of the reference and two phase modulated sawtooth waveforms, as:

$$p_d(t) = f(t) + \mathrm{st}(\omega_c t - (\pi/2)[1+f(t)] + \pi) - \mathrm{st}(\omega_c t + (\pi/2)[1+f(t)] - \pi) \quad (1)$$

where the two sawtooth waveforms are defined in terms of a general periodic sawtooth function $\mathrm{st}(\theta)$, where:

$$\mathrm{st}(\theta) = \theta/\pi, \quad \text{for } -\pi \le \theta < +\pi, \quad \text{and:}$$
$$\mathrm{st}(\theta \pm 2k\pi) = \mathrm{st}(\theta), \quad \text{for } k = 1,2,3,\ldots,\infty \quad (2)$$

This general sawtooth function can be expanded as an exponential Fourier series according to:

$$\mathrm{st}(\theta) = \frac{j}{\pi} \sum_{m=-\infty, m\neq 0}^{\infty} \frac{1}{m} e^{jm(\theta+\pi)} \quad (3)$$

Substituting (3) into (1) yields after a little algebra [18]:

$$p_d(t) = f(t) + \sum_{m=-\infty, m\neq 0}^{\infty} \frac{j}{m\pi} e^{jm\omega_c t} e^{-j\frac{\pi}{2}[1+f(t)]} - \sum_{m=-\infty, m\neq 0}^{\infty} \frac{j}{m\pi} e^{jm\omega_c t} e^{j\frac{\pi}{2}[1+f(t)]} \quad (4)$$

which can be further simplified to:

$$p_d(t) = f(t) + \sum_{\substack{m=-\infty \\ m\neq 0}}^{\infty} \frac{2}{m\pi} e^{jm\omega_c t} \sin\left(m\frac{\pi}{2}[1+f(t)]\right) \quad (5)$$

Taking the Fourier transform of $p_d(t)$ yields [18]:

$$P_d(\omega) = F(\omega) + \sum_{m=-\infty, m\neq 0}^{\infty} \int_{-\infty}^{\infty} \frac{2}{m\pi} \sin\left(m\frac{\pi}{2}[1+f(t)]\right) e^{-j(\omega - m\omega_c)t} dt \quad (6)$$

Equations (5) and (6) show that the PWM pulse train includes a copy of the reference $f(t)$, and a series of carrier and sideband harmonic groups, generated from the basis function, $\sin(m[\pi/2][1+f(t)])$, which via the $e^{jm\omega_c t}$ product terms are frequency shifted to be centred around $\omega = m\omega_c$.

To apply these concepts to multilevel PWM, consider the Phase Disposition (PD) PWM strategy illustrated in Fig.

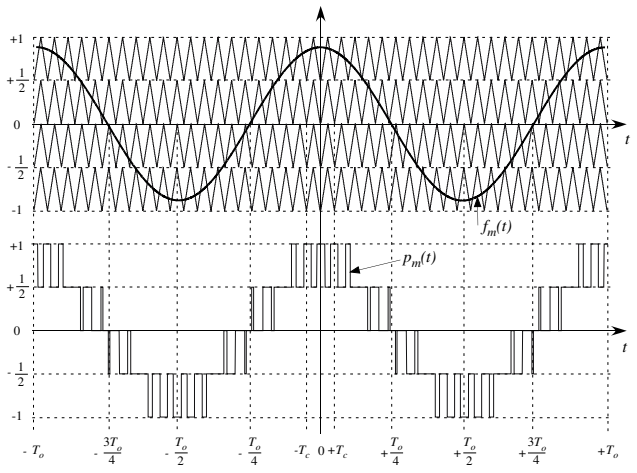

Fig. 2: Five level Phase Disposition (PD) PWM process.

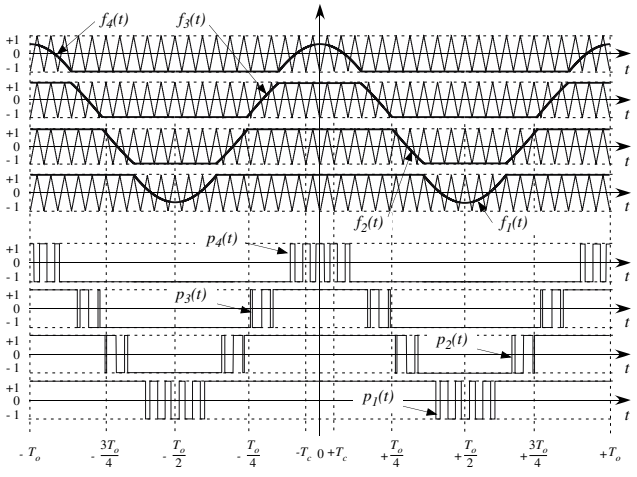

Fig. 3: Separation into discontinuous PD references and pulse trains.

TABLE I : Discontinuous Reference Waveforms for 3 and 5 Level PD PWM – For sinusoidal PWM $\psi = cos^{-1}(1/2M)$.

	Regions within $-\pi \le \omega_o t \le +\pi$		$f_1(t)$	$f_2(t)$	$f_3(t)$	$f_4(t)$
3 Level	$-\pi/2 \le \omega_o t \le +\pi/2$	-	$+1$	$2f_m(t)-1$	-	-
	$-\pi \le \omega_o t \le -\pi/2$	$+\pi/2 \le \omega_o t \le +\pi$	$2f_m(t)+1$	-1	-	-
5 Level	$-\psi \le \omega_o t \le +\psi$	-	$+1$	$+1$	$+1$	$4f_m(t)-3$
	$-\pi/2 \le \omega_o t \le -\psi$	$+\psi \le \omega_o t \le +\pi/2$	$+1$	$+1$	$4f_m(t)-1$	-1
	$-(\pi-\psi) \le \omega_o t \le -\pi/2$	$+\pi/2 \le \omega_o t \le +(\pi-\psi)$	$+1$	$4f_m(t)+1$	-1	-1
	$-\pi \le \omega_o t \le -(\pi-\psi)$	$+(\pi-\psi) \le \omega_o t \le +\pi$	$4f_m(t)+3$	-1	-1	-1

2. This is recognised as the optimal three phase PWM strategy [13][14], and compares a single reference $f_m(t)$ to multiple triangular carriers arranged in contiguous bands to generate the multilevel pulse train $p_m(t)$. For inverters with redundant phase voltage states (e.g. cascaded inverters) the pulse train must be decoded to generate gate signals, but as this does not affect the spectral content of the multilevel waveform this issue will not be considered in this paper.

Application of the one-dimensional spectral analysis strategy begins by deconstructing the multilevel reference and pulse train into discontinuous references $(\text{i.e. } f_1(t) \text{ to } f_4(t))$ and discrete two-level pulse trains $(\text{i.e. } p_1(t) \text{ to } p_4(t))$ associated with each disposition band, as shown in Fig. 3. Observe that the references and pulse trains have been level shifted and normalised to extend across the range [-1:+1] to enable the usage of (5). These discontinuous references, and their regions of discontinuity, can be defined in terms of the overall multilevel reference $f_m(t)$, as shown for three and five level systems in Table I. The continuous section of each function is easily generalised for N-levels as:

$$f_k(t) = (N-1)f_m(t) + (N-2k), \quad \text{for } k = 1,\ldots,N-1 \tag{7}$$

with discontinuous regions defined by:

$$f_k(t_k) = \pm 1 \tag{8}$$

Substituting (7) into (6) and summing across all disposition bands yields the multilevel PWM spectrum as:

$$P_m(\omega) = \frac{1}{N-1}\sum_{k=1}^{N-1} P_k(\omega) = \frac{1}{N-1}\sum_{k=1}^{N-1}\left\{ F_k(\omega) + \sum_{m=-\infty, m\neq 0}^{\infty} \int_{-\infty}^{\infty} \frac{2}{m\pi} \sin\left(m\frac{\pi}{2}[1+f_k(t)] \right) e^{-j(\omega - m\omega_c)t} dt \right\} \tag{9}$$

where the k summation accounts for the superposition across multiple disposition bands but is not associated with a two-dimensional series. Note also that in (9) all carriers have the same phase. However an arbitrary phase shift, ϕ_k, can be set for any carrier by substituting $\omega_c t \Rightarrow \omega_c t + \phi_k$ into the sideband generator function associated with $p_k(t)$, which from (9) results in the additional sideband product term $e^{jm\phi_k}$. This simple operation enables the analysis of PWM strategies such as the Phase Opposition Disposition (POD) (i.e. all carriers above zero are phase shifted by $180°$ relative to the carriers below zero) and the Alternative Phase Opposition Disposition (APOD) (i.e. every carrier is $180°$ out of phase with its neighbouring carrier) methods [13][15]. While POD and APOD are well known to be sub-optimal compared to PD PWM for three phase applications, they are still effective for single phase inverters. Furthermore APOD is equivalent to phase shifted PWM, which is commonly employed with cascaded and modular multilevel converters (MMCs) [13][15][11].

III. Modification for Sampling Effects and Periodic Reference Waveforms.

Digital PWM implementations require a sampled reference. Typically symmetric (one sample per carrier period) or asymmetric (two samples per carrier period) regular sampling [1] will be used, with the sampling instants matched to the carrier peak and/or trough as shown for asymmetric PD PWM in Fig. 4. While straight forward to implement, the spectral analysis of regularly sampled multilevel PWM remains an open problem in modulation theory, with the only published results based on numerical solution of the double Fourier integral [14]. However as shown in [18], sampling is readily incorporated into the one-dimensional spectral analysis approach. The key is to recognise that sampling is equivalent to multiplying the sideband basis functions by an impulse train with a period equal to the sampling rate, followed by convolution with a Zero-Order-Hold (ZOH) filter response [2]. While the algebraic steps associated with this process are considerable, the multilevel case follows the same essential process as for two-level PWM (see section IV, pp. 4 – 8 of [18]), and so the development is omitted from this paper due to space

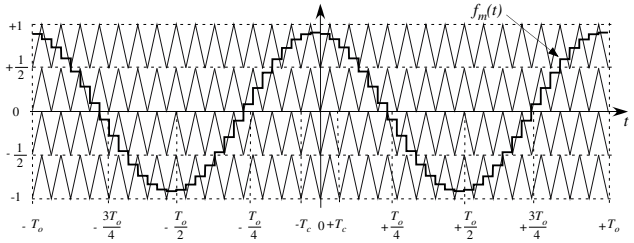

Fig. 4: Asymmetric regularly sampled PD PWM.

considerations. The resulting Fourier transforms of the multilevel pulse train for symmetric and asymmetric regularly sampled PWM are hence defined as:

$$P_m(\omega)=\frac{1}{N-1}\sum_{k=1}^{N-1}\sum_{m=-\infty}^{\infty}\left\{\frac{2\omega_c}{\pi\omega}\times \int_{-\infty}^{\infty}\sin\left(\frac{\omega}{\omega_c}\frac{\pi}{2}\left[1+f_k(t)\right]\right)e^{-j(\omega-m\omega_c)t}dt\right\} \quad (10)$$

$$P_m(\omega)=\frac{1}{N-1}\sum_{k=1}^{N-1}\sum_{m=-\infty}^{\infty}\left\{\frac{2\omega_c}{\pi\omega}\times \int_{-\infty}^{\infty}\sin\left(\frac{\pi}{2}\left[m+\frac{\omega}{\omega_c}f_k(t)\right]\right)e^{-j(\omega-m\omega_c)t}dt\right\} \quad (11)$$

for symmetric and asymmetric PWM respectively.

A comparison of (9), (10) and (11) reveals that the integral in each transform has the same form, viz.:

$$S_m(\omega)=\int_{-\infty}^{\infty}\alpha(\omega)\sin(\beta(\omega)+\gamma(\omega)f(t))e^{-j(\omega-m\omega_c)t}dt \quad (12)$$

where the $\alpha(\omega)$, $\beta(\omega)$ and $\gamma(\omega)$ parameters for each sampling variation are detailed in Table II. While the integral in (12) is valid for general reference waveforms, a particularly important group is for periodic references. Under these conditions the $\sin(\beta(\omega)+\gamma(\omega)f(t))$ sideband basis function can be expanded as an exponential Fourier series, which upon substitution into the integral of (12) results in the following simplified Fourier transform [18]:

$$S_m(\omega)=\sum_{n=-\infty}^{\infty}(\pi\alpha(\omega_{mn})/j)\times \left[C_{mn}(\omega_{mn})e^{j\beta(\omega_{mn})}-\overline{C}_{m(-n)}(\omega_{mn})e^{-j\beta(\omega_{mn})}\right]\delta(\omega-\omega_{mn}) \quad (13)$$

where $\omega_{mn}=m\omega_c+n\omega_o$, and:

$$C_{mn}(\omega)=\frac{1}{2\pi}\int_{-\pi}^{+\pi}e^{j\gamma(\omega)f(t)}e^{-jn\omega_o t}d(\omega_o t) \quad (14)$$

The analytic result for periodic references hence reduces to evaluation of the one-dimensional Fourier integral in (14), substitution of the C_{mn} into (13), and superposition across all disposition bands via (9), (10) or (11) as is appropriate for a specified sampling strategy.

TABLE II : $\alpha(\omega)$, $\beta(\omega)$, $\gamma(\omega)$ Values for Different Sampling Methods

Sampling Method	$\alpha(\omega)$	$\beta(\omega)$	$\gamma(\omega)$
Naturally Sampled	$\frac{2}{m\pi}$	$\frac{m\pi}{2}$	$\frac{m\pi}{2}$
Symmetric Regular Sampled	$\frac{2}{\pi}\frac{\omega_c}{\omega}$	$\frac{\pi}{2}\frac{\omega}{\omega_c}$	$\frac{\pi}{2}\frac{\omega}{\omega_c}$
Asymmetric Regular Sampled	$\frac{2}{\pi}\frac{\omega_c}{\omega}$	$\frac{\pi}{2}m$	$\frac{\pi}{2}\frac{\omega}{\omega_c}$

IV. SELECTED ANALYTIC RESULTS

To demonstrate the one-dimensional spectral analysis strategy, selected analytic results for three and five level inverters will now be developed. For each of the results that follow, the phase voltage is defined as the potential difference between a switched phase leg relative to a virtual earth (i.e. the mid-point of a split DC link), while the line to line voltage is the potential difference between two switched phase legs. These definitions are illustrated in Fig. 5, which also shows example Neutral Point Clamped (NPC) and flying capacitor three level phase leg networks. All of the results that follow will be developed for a normalized DC link voltage (i.e. $V_{DC}=1$), but correction for an arbitrary DC link value is readily achieved by multiplying by the factor V_{DC}.

A. *Three Level PD PWM.*

Analysis of three level PD PWM requires evaluation of the Fourier integral in (14) for the upper and lower PWM references (i.e. $f_2(t)$ and $f_1(t)$) considering an overall PD reference of $f_m(t)=M\cos(\omega_o t)$. From Table I, this yields a pair of Fourier integrals, as shown in (15) and (16) at the top of the page. Observe that the discontinuous nature of $f_2(t)$ and $f_1(t)$ has split the integral of (14) into three sub-integrals with integration limits defined by the boundaries in Table I. This pattern occurs with all multilevel cases. To proceed now requires Jacobi-Anger expansions of the form:

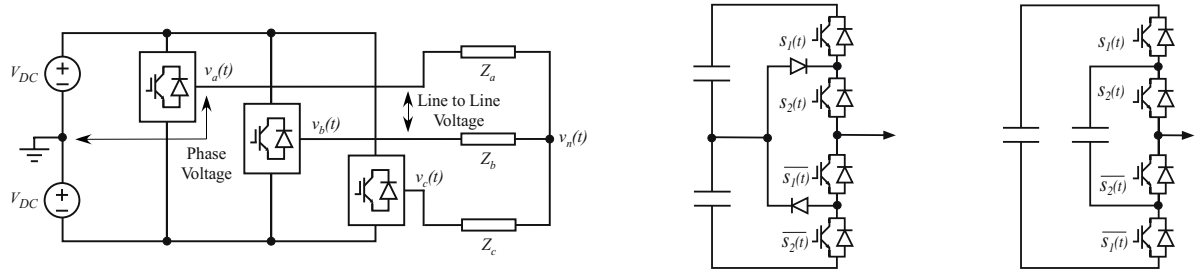

(a) General three phase multilevel inverter topology.

(b) (NPC) phase leg

(c) Flying capacitor phase leg.

Fig. 5: Multilevel inverter topology, showing the definition of the phase and line to line switched voltages, and example three level phase leg structures.

$$C_{mn\_2}(\omega)=\frac{1}{2\pi}\left[\int_{-\pi}^{-\frac{\pi}{2}} e^{-j\gamma(\omega)}e^{-jn\omega_o t}d(\omega_o t)+\int_{-\frac{\pi}{2}}^{\frac{\pi}{2}} e^{j\gamma(\omega)(2M\cos(\omega_o t)-1)}e^{-jn\omega_o t}d(\omega_o t)+\int_{\frac{\pi}{2}}^{\pi} e^{-j\gamma(\omega)}e^{-jn\omega_o t}d(\omega_o t)\right] \quad (15)$$

$$C_{mn\_1}(\omega)=\frac{1}{2\pi}\left[\int_{-\pi}^{-\frac{\pi}{2}} e^{j\gamma(\omega)(2M\cos(\omega_o t)+1)}e^{-jn\omega_o t}d(\omega_o t)+\int_{-\frac{\pi}{2}}^{\frac{\pi}{2}} e^{j\gamma(\omega)}e^{-jn\omega_o t}d(\omega_o t)+\int_{\frac{\pi}{2}}^{\pi} e^{j\gamma(\omega)(2M\cos(\omega_o t)+1)}e^{-jn\omega_o t}d(\omega_o t)\right] \quad (16)$$

$$C_{mn\_2}(\omega)=\frac{1}{2\pi}\left[\int_{\frac{\pi}{2}}^{\frac{3\pi}{2}} e^{-j\gamma(\omega)}e^{-jn\omega_o t}d(\omega_o t)+\sum_{k=-\infty}^{\infty} j^k J_k(2\gamma(\omega)M)e^{-j\gamma(\omega)}\int_{-\frac{\pi}{2}}^{\frac{\pi}{2}} e^{j[k-n]\omega_o t}d(\omega_o t)\right] \quad (18)$$

$$C_{mn\_1}(\omega)=\frac{1}{2\pi}\left[\int_{-\frac{\pi}{2}}^{\frac{\pi}{2}} e^{+j\gamma(\omega)}e^{-jn\omega_o t}d(\omega_o t)+\sum_{k=-\infty}^{\infty} j^k J_k(2\gamma(\omega)M)e^{+j\gamma(\omega)}\int_{\frac{\pi}{2}}^{\frac{3\pi}{2}} e^{j[k-n]\omega_o t}d(\omega_o t)\right] \quad (19)$$

$$e^{j\gamma(\omega)\lambda M\cos(\omega_o t)}=\sum_{k=-\infty}^{\infty} j^k J_k(\gamma(\omega)\lambda M)e^{jk\omega_o t} \quad (17)$$

where $J_k(x)$ denotes a Bessel function of the first kind, order k and argument x. Substitution of (17) into (15) and (16) yields an infinite summation of integral expressions involving simple sinusoids, as shown in (18) and (19) at the bottom of the page. Note here that integral transforms have been applied to group terms that repeat with a 2π periodicity. The phase voltage spectrum can now be derived by evaluating the integrals in (18) and (19), substituting the results into (13) and then summing the contributions from both references in accordance with (9), (10) and (11). For symmetric and asymmetric regular sampling, this yields:

$$\begin{aligned} V_a(\omega)=&\sum_{m=-\infty,m\neq 0}^{\infty}\Lambda_{m0}\,\delta(\omega-m\omega_c)\\ &+\sum_{m=-\infty}^{\infty}\sum_{n=-\infty,n\neq 0}^{\infty}\Lambda_{mn}\,\delta(\omega-m\omega_c-n\omega_o)\end{aligned} \quad (20)$$

where the first summation group in (20) are the carrier harmonics, and the second group includes carrier sidebands when $m\neq 0$, and the fundamental and baseband terms when $m=0$.The spectral coefficients Λ_{m0} and Λ_{mn} are defined according to (21) and (22), shown at the top of the next page. Note that the ν_{mn} μ_{mn}, χ_{mn} and ξ_{mn} factors in (21) and (22) depend on the sampling strategy according to:

$$\begin{aligned}\nu_{mn}=&\sin(\beta(\omega_{mn})-\gamma(\omega_{mn}))\\ &+\cos(n\pi)\sin(\beta(\omega_{mn})+\gamma(\omega_{mn}))\end{aligned} \quad (23)$$

$$\begin{aligned}\mu_{mn}=&\sin(\beta(\omega_{mn})-\gamma(\omega_{mn})+k\,\pi/2)\\ &-\cos(n\pi)\sin(\beta(\omega_{mn})+\gamma(\omega_{mn})+k\,\pi/2)\end{aligned} \quad (24)$$

$$\begin{aligned}\chi_{mn}=&\sin(\beta(\omega_{mn})-\gamma(\omega_{mn})+n\,\pi/2)\\ &+\cos(n\pi)\sin(\beta(\omega_{mn})+\gamma(\omega_{mn})-n\,\pi/2)\end{aligned} \quad (25)$$

$$\begin{aligned}\xi_{mn}=&\sin(\beta(\omega_{mn})-\gamma(\omega_{mn})+k\,\pi/2)\\ &+\cos(n\pi)\sin(\beta(\omega_{mn})+\gamma(\omega_{mn})-k\,\pi/2)\end{aligned} \quad (26)$$

Equations (20) through (22) represent the closed form analytic spectrum produced by a three level regularly sampled modulator, reported for the first time in this paper.

For the naturally sampled case, (20) must be re-defined to separate the fundamental from the second summation term according to:

$$\begin{aligned}V_a^{\text{nat}}(\omega)=&\pi M(\delta(\omega+\omega_o)+\delta(\omega-\omega_o))\\ &+\sum_{\substack{m=-\infty\\ m\neq 0}}^{\infty}\Lambda_{m0}^{\text{nat}}\,\delta(\omega-\omega_{m0})+\sum_{\substack{m=-\infty\\ m\neq 0}}^{\infty}\sum_{\substack{n=-\infty\\ n\neq 0}}^{\infty}\Lambda_{mn}^{\text{nat}}\,\delta(\omega-\omega_{mn})\end{aligned} \quad (27)$$

The $\Lambda_{m0}^{\text{nat}}$ and $\Lambda_{mn}^{\text{nat}}$ coefficients in (27) are readily derived from (21) and (22) upon substitution of the naturally sampled forms for $\alpha(\omega)$, $\beta(\omega)$ and $\gamma(\omega)$ from Table II, yield the coefficients given in (28) and (29). Careful examination of (27), (28) and (29) reveals that the naturally sampled three level PD analytic results are equivalent to Eq. (11.37) of [1], which therefore validates the analytic procedure outlined in this paper.

$$\Lambda_{m0}=\frac{\alpha(\omega_{m0})}{N-1}\left[\pi(1+J_0(2\gamma(\omega)M))\nu_{mn}+\sum_{k=1}^{\infty}\frac{4}{k}J_k(2\gamma(\omega)M)\sin(k\,\pi/2)\mu_{mn}\right] \quad (21)$$

$$\Lambda_{mn}=\frac{\alpha(\omega_{mn})}{N-1}\left[\begin{aligned}&(2/n)\sin(n\,\pi/2)[\cos(n\pi)+J_0(2\gamma(\omega)M)]\nu_{mn}+\pi J_n(2\gamma(\omega)M)\chi_{mn}\\ &+\sum_{k=1,\,k\neq|n|}^{\infty}2J_k(2\gamma(\omega)M)\left[\frac{\sin((n-k)\pi/2)}{n-k}+\frac{\sin((n+k)\pi/2)}{n+k}\right]\xi_{mn}\end{aligned}\right] \quad (22)$$

$$\Lambda_{m0}^{\text{nat}} = \frac{2}{m\pi}\frac{\left[1-\cos\left((m+n)\pi\right)\right]}{(N-1)}\sum_{k=0}^{\infty}\frac{4}{2k+1}J_{2k+1}\left(2\gamma(\omega)M\right) \tag{28}$$

$$\Lambda_{mn}^{\text{nat}} = \frac{2}{m\pi}\frac{\left[1-\cos\left((m+n)\right)\pi\right]}{N-1}\left[\pi J_n\left(2\gamma(\omega)M\right)\sin\left(n\frac{\pi}{2}\right) - \sum_{k=0,\ 2k+1\neq|n|}^{\infty}4J_{2k+1}\left(2\gamma(\omega)M\right)\left[\frac{(2k+1)\cos(n\pi/2)}{(n-2k-1)(n+2k+1)}\right]\right] \tag{29}$$

B. Three Level APOD PWM.

The generality of the one-dimensional spectral analysis approach can be shown by developing analytic solutions for the three level APOD strategy. APOD PWM uses the same reference waveforms as PD PWM, but with upper and lower carrier phase shifts of 0° and 180° respectively. Hence the Fourier integral for the upper APOD reference $f_2(t)$ is identical to the PD case as shown in (18), while the Fourier integral for the lower APOD reference $f_1(t)$ is the same as (19) but multiplied by the factor $e^{jm\pi}$ to account for the 180° lower carrier phase shift.

Hence the process for developing the APOD phase voltage spectrum is identical to the PD case, and yields the same expression as shown in (20), with the same coefficients as detailed in (21) and (22), albeit with different ν_{mn}, μ_{mn}, χ_{mn} and ξ_{mn} factors, which for the APOD case are defined as:

$$\begin{aligned}\nu_{mn} &= \sin\left(\beta(\omega_{mn})-\gamma(\omega_{mn})\right)\\ &\quad+\cos\left([m+n]\pi\right)\sin\left(\beta(\omega_{mn})+\gamma(\omega_{mn})\right)\end{aligned} \tag{30}$$

$$\begin{aligned}\mu_{mn} &= \sin\left(\beta(\omega_{mn})-\gamma(\omega_{mn})+k\,\pi/2\right)\\ &\quad-\cos\left([m+n]\pi\right)\sin\left(\beta(\omega_{mn})+\gamma(\omega_{mn})+k\,\pi/2\right)\end{aligned} \tag{31}$$

$$\begin{aligned}\chi_{mn} &= \sin\left(\beta(\omega_{mn})-\gamma(\omega_{mn})+n\,\pi/2\right)\\ &\quad+\cos\left([m+n]\pi\right)\sin\left(\beta(\omega_{mn})+\gamma(\omega_{mn})-n\,\pi/2\right)\end{aligned} \tag{32}$$

$$\begin{aligned}\xi_{mn} &= \sin\left(\beta(\omega_{mn})-\gamma(\omega_{mn})+k\,\pi/2\right)\\ &\quad+\cos\left([m+n]\pi\right)\sin\left(\beta(\omega_{mn})+\gamma(\omega_{mn})-k\,\pi/2\right)\end{aligned} \tag{33}$$

Equations (20) to (22), and (30) to (33) represent the closed form analytic spectrum produced by a three level regularly sampled APOD modulator. Substitution of the naturally sampled conditions from Table II into (30) to (33) enables considerable simplification of these factors. This yields a naturally sampled APOD phase voltage solution as:

$$\begin{aligned}V_a^{\text{nat}}(\omega) &= \pi M\left(\delta(\omega+\omega_o)+\delta(\omega-\omega_o)\right)\\ &\quad+\sum_{\substack{m=-\infty\\ m\neq 0}}^{\infty}\sum_{n'=-\infty}^{\infty}\Lambda_{m(2n'-1)}^{\text{nat}}\,\delta\left(\omega-m\omega_c-(2n'-1)\omega_o\right)\end{aligned} \tag{34}$$

$$\Lambda_{m(2n'-1)}^{\text{nat}} = \frac{2}{m}\cos\left((n'-1)\pi\right)J_{2n'-1}\left(m\pi M\right) \tag{35}$$

Careful examination of (34) and (35) reveals that the naturally sampled three level APOD analytic results are equivalent to Eq. (3) of [15] and Eq. (11.41) of [1], again providing confidence in the one dimensional spectral analysis strategy proposed in this paper.

C. Five Level PD PWM.

Development of analytic results for higher order systems follows the same general procedure as detailed for three level PWM above, but must also account for the increased number of disposition bands. To illustrate, consider a five level PD modulator, again with the overall reference defined as $f_m(t) = M\cos(\omega_o t)$, and with individual disposition

$$C_{mn\_4}(\omega) = \frac{1}{2\pi}\left[\int_{-\pi}^{-\psi}e^{-j\gamma(\omega)}e^{-jn\omega_o t}d(\omega_o t)+\int_{-\psi}^{\psi}e^{j\gamma(\omega)(4M\cos(\omega_o t)-3)}e^{-jn\omega_o t}d(\omega_o t)+\int_{\psi}^{\pi}e^{-j\gamma(\omega)}e^{-jn\omega_o t}d(\omega_o t)\right] \tag{36}$$

$$C_{mn\_3}(\omega) = \frac{1}{2\pi}\left[\begin{aligned}&\int_{-\pi}^{-\frac{\pi}{2}}e^{-j\gamma(\omega)}e^{-jn\omega_o t}d(\omega_o t)+\int_{-\frac{\pi}{2}}^{-\psi}e^{j\gamma(\omega)(4M\cos(\omega_o t)-1)}e^{-jn\omega_o t}d(\omega_o t)+\int_{-\psi}^{\psi}e^{j\gamma(\omega)}e^{-jn\omega_o t}d(\omega_o t)\\ &+\int_{\psi}^{\frac{\pi}{2}}e^{j\gamma(\omega)(4M\cos(\omega_o t)-1)}e^{-jn\omega_o t}d(\omega_o t)+\int_{\frac{\pi}{2}}^{\pi}e^{-j\gamma(\omega)}e^{-jn\omega_o t}d(\omega_o t)\end{aligned}\right] \tag{37}$$

$$C_{mn\_2}(\omega) = \frac{1}{2\pi}\left[\begin{aligned}&\int_{-\pi}^{-\pi+\psi}e^{-j\gamma(\omega)}e^{-jn\omega_o t}d(\omega_o t)+\int_{-\pi+\psi}^{-\frac{\pi}{2}}e^{j\gamma(\omega)(4M\cos(\omega_o t)+1)}e^{-jn\omega_o t}d(\omega_o t)+\int_{-\frac{\pi}{2}}^{\frac{\pi}{2}}e^{j\gamma(\omega)}e^{-jn\omega_o t}d(\omega_o t)\\ &+\int_{\frac{\pi}{2}}^{\pi-\psi}e^{j\gamma(\omega)(4M\cos(\omega_o t)+1)}e^{-jn\omega_o t}d(\omega_o t)+\int_{\pi-\psi}^{\pi}e^{-j\gamma(\omega)}e^{-jn\omega_o t}d(\omega_o t)\end{aligned}\right] \tag{38}$$

$$C_{mn\_1}(\omega) = \frac{1}{2\pi}\left[\int_{-\pi}^{-\pi+\psi}e^{j\gamma(\omega)(4M\cos(\omega_o t)+3)}e^{-jn\omega_o t}d(\omega_o t)+\int_{-\pi+\psi}^{\pi-\psi}e^{j\gamma(\omega)}e^{-jn\omega_o t}d(\omega_o t)+\int_{\pi-\psi}^{\pi}e^{j\gamma(\omega)(4M\cos(\omega_o t)+3)}e^{-jn\omega_o t}d(\omega_o t)\right] \tag{39}$$

$$V_a^{\text{nat}}(\omega)=\Bigg\{\pi M\left(\delta(\omega+\omega_o)+\delta(\omega-\omega_o)\right)+\sum_{m=-\infty}^{\infty}\Lambda_{(2m+1)(0)}^{\text{nat}}\,\delta(\omega-(2m+1)\omega_c)$$
$$+\sum_{m=-\infty}^{\infty}\sum_{n=-\infty,n\neq 0}^{\infty}\Lambda_{(2m+1)(2n)}^{\text{nat}}\,\delta(\omega-(2m+1)\omega_c-(2n)\omega_o)+\sum_{m=-\infty,m\neq 0}^{\infty}\sum_{n=-\infty}^{\infty}\Lambda_{(2m)(2n-1)}^{\text{nat}}\,\delta(\omega-(2m)\omega_c-(2n-1)\omega_o)\Bigg\} \tag{41}$$

$$\Lambda_{(2m+1)(0)}^{\text{nat}}=\frac{2}{\pi}\frac{1}{(N-1)(2m+1)}\sum_{k=0}^{\infty}\frac{8J_{2k+1}((2m+1)2\pi M)}{2k+1}\left[1-2\sin((2k+1)\psi)\cos(k\pi)\right] \tag{42}$$

$$\Lambda_{(2m)(2n-1)}^{\text{nat}}=\frac{2}{\pi}\frac{2}{(N-1)(2m)}J_{2n-1}(4m\pi M)\cos((n-1)\pi) \tag{43}$$

$$\Lambda_{(2m+1)(2n)}^{\text{nat}}=\frac{2}{\pi}\frac{1}{(N-1)(2m+1)}\sum_{k=0}^{\infty}\Bigg\{\begin{bmatrix}4J_{2k+1}((2m+1)2\pi M)\cos(k\pi)\times\\ \left[\frac{\cos((k-n)\pi)-2\sin((2k+1-2n)\psi)}{(2k+1-2n)}+\frac{\cos((k+n)\pi)-2\sin((2k+1+2n)\psi)}{(2k+1+2n)}\right]\end{bmatrix}\Bigg\} \tag{44}$$

references detailed in Table I. Substitution of each reference into (14) produces four separate integral expressions for each disposition band, as shown in (36) to (39) at the bottom of the page. As with the three level case, each integral is broken up into discrete sections due to the discontinuous nature of the disposition reference waveforms, with the integration limits defined by the boundaries in Table I. Note that the angle ψ is defined as:

$$\psi=\cos^{-1}(1/(2M)) \tag{40}$$

Evaluation of the integral expressions in (36) to (39) requires substitution of the Jacobi-Anger series of (17), which yields an infinite summation of integrals involving simple sinusoids. While the resulting integrals are readily solved using elementary techniques, the ultimate solutions developed are particularly complex for the symmetric and asymmetric regularly sampled cases. This is caused by the production of non-trivial sampling factors (i.e. the equivalent to the ν_{mn} μ_{mn}, χ_{mn} and ξ_{mn} from the three level solution) which do not readily simplify. Accordingly these solutions have not been included in this paper due to space considerations, but they have been used to calculate the theoretical regularly sampled five level spectral results shown in section V.

To validate the analytic methodology, the naturally sampled five level PD solution is derived by substituting the associated $\alpha(\omega)$, $\beta(\omega)$ and $\gamma(\omega)$ values from Table II into the developed five level regularly sampled solution. This produces a phase voltage expression as shown in (41), where the sideband harmonics have been separated into odd *m*/even *n*, and even *m*/odd *n* groups, with coefficients given in (42), (43) and (44). Examination of these expressions reveals that they are equivalent to previously published five level PD spectral results, including equations (21) to (24) of [14], equation (4) of [15], and equation (11.45) of [1]. Combined with the three level analysis, these results confirm the validity of the one-dimensional spectral analysis strategy.

V. Theoretical Spectral Performance

The theoretical spectral performance of the three and five level PD modulators have been calculated using MATLAB, based on the analytical results developed in section IV. The calculation methodology is to construct a frequency vector that spans the frequency range of interest. A loop structure is then used to search through the frequency vector to find integer combinations of the *m* and *n* indices for each frequency according to $\omega_{mn}=m\omega_c+n\omega_o$. Once these values have been identified, the harmonic amplitudes are readily calculated using either (21) and (22), (28) and (29), or (42) to (44), depending on which type of strategy is being considered. Note that the Bessel functions within these coefficients are readily computed using the standard `besselj(n,x)` MATLAB function. The PWM conditions considered are for a modulation depth of $M=0.9$ and carrier and fundamental frequencies of 2100Hz and 50Hz. These conditions have been selected so as to enable comparison to previously published and experimentally validated spectral results as shown in [14] and chapter 11 of [1]. FFT spectral results obtained using time domain switched simulations performed within MATLAB have also been used to provide an immediate confirmation of the calculated analytic spectral results.

Fig. 8 and Fig. 7 compare the theoretical three level PD PWM phase and line to line voltage spectra, and an FFT of the simulated line to line voltage, for naturally and asymmetric regularly sampled PWM conditions. Fig. 8 clearly matches the well-known PD spectral results (e.g. Fig. 11.15 of [1]), with the formation of a large carrier harmonic in the phase voltage which cancels, along with triplen sidebands, in the line to line voltage. Fig. 7 reveals the theoretical impact of asymmetric regular sampling with the formation of a baseband group at 10^{-3} magnitude extending up into the first sideband region, as well as sideband asymmetry which is a well-known outcome for regularly sampled two-level modulators.

Fig. 6 and Fig. 9 show the theoretical five level PD PWM phase and line to line voltage spectra, and matching

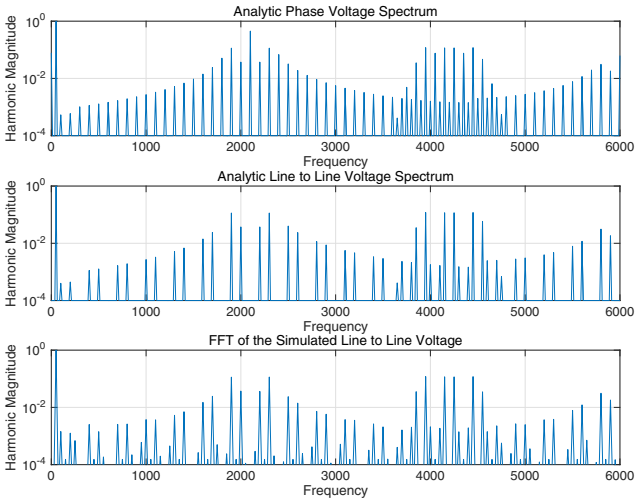

Fig. 8: Three level PD spectrum, natural sampling, *M=0.9, fo = 50Hz, fc = 2100Hz.*

FFT spectral results for the simulated switched line to line voltage, again considering natural and asymmetric regularly sampled conditions. Just as with the three level results, these spectral plots clearly match previously published results, in particular Figs. 3 to 8 of [14]. Again the signatures of PD PWM are evident, with the formation of the large carrier harmonic in the phase voltage spectrum which cancels along with triplen sidebands in the line to line voltage. However, in contrast to the three level case the effects of regular sampling in the baseband region are much less significant, with a smaller group of harmonics at the 10^{-3} magnitude level, and less pronounced sideband asymmetry. These theoretical results suggest that the spectral impact of regular sampling may be diminished for typical pulse ratios and for systems with a higher number of levels, and as such the naturally sampled spectral results are most likely sufficient for practical spectral characterisation purposes.

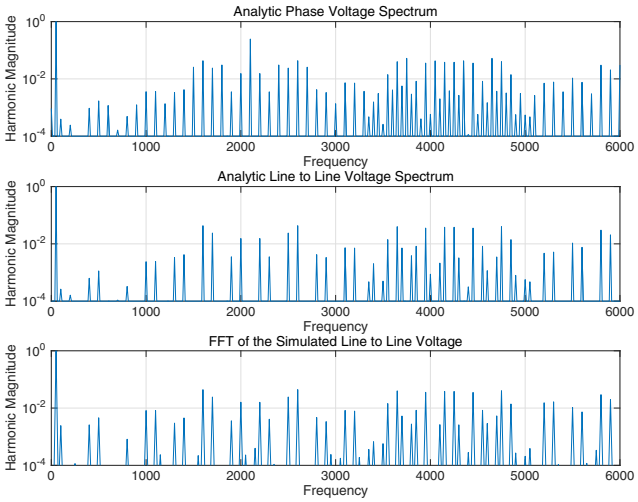

Fig. 6: Five level PD spectrum, natural sampling, *M=0.9, fo = 50Hz, fc = 2100Hz.*

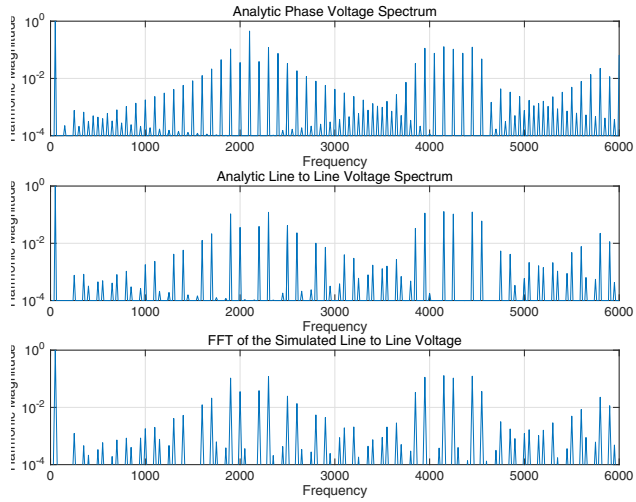

Fig. 7: Three level PD spectrum, asymmetric regular sampling, *M=0.9, fo = 50Hz, fc = 2100Hz.*

VI. Numerical Spectral Characterisation

For PWM strategies such as multilevel centred space vector modulation as proposed in [17], substantial difficulties still remain in attempting to develop closed form analytic solutions using the methodology outlined in section IV. This is because the reference waveforms employed with these strategies are non-trivial and include sharp modulation depth dependent discontinuities that are difficult to describe in terms of simple trigonometric functions. To illustrate, recall that a multilevel centred space vector reference waveform includes two offsets [17], the first being a third harmonic component to ensure full utilization of the linear modulation range of the converter, viz.:

$$V_x^{'} = V_x - \left[\max\left(V_a, V_b, V_c\right) + \min\left(V_a, V_b, V_c\right)\right]/2 \qquad (45)$$

for $x \in \{a, b, c\}$. The second offset is a modulo function to

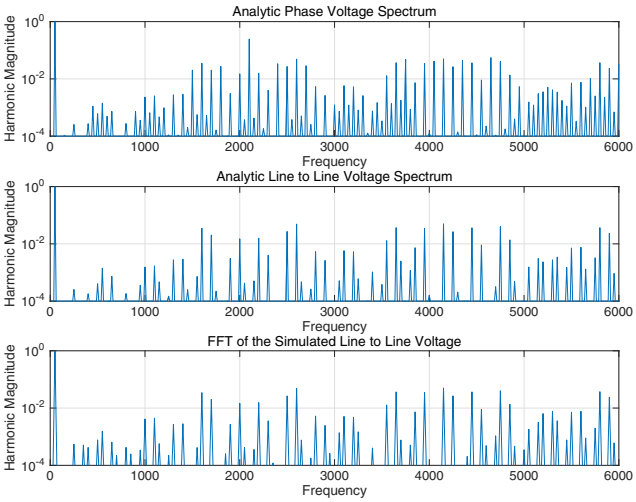

Fig. 9: Five level PD spectrum, asymmetric regular sampling, *M=0.9, fo = 50Hz, fc = 2100Hz.*

$$P_m\left(\kappa\frac{2\pi}{N_sT_s}\right)=\frac{1}{N-1}\sum_{k=1}^{N-1}\left\{\sum_{\eta=0}^{N_s-1}f_k(\eta T_s)e^{-j2\pi\eta\kappa/N_s}+\sum_{m=-\infty,\,m\neq 0}^{\infty}\sum_{\eta=0}^{N_s-1}\frac{2}{m\pi}\sin\left(m\frac{\pi}{2}\left[1+f_k(\eta T_s)\right]\right)e^{jm\omega_c\eta T_s}\,e^{-j2\pi\eta\kappa/N_s}\right\} \quad (48)$$

identify the first and last switching edge within a half-carrier equivalent interval required for vector centering, viz.:

$$V_x^{''}=\left[V_x^{'}+1\right]\text{modulo}\left(2/(N-1)\right) \quad (46)$$

The final references incorporating both offsets are:

$$f_{m\_x}(\omega_o t)=V_x^{'}+1-\frac{\max\left(V_a^{''},V_b^{''},V_c^{''}\right)+\min\left(V_a^{''},V_b^{''},V_c^{''}\right)}{2} \quad (47)$$

While such reference waveforms are not easily incorporated into the Fourier integral of (14), accurate spectral results can be obtained by numerically computing the Fourier transforms in (9), (10) or (11). This is achieved by first computing the integrand function of the Fourier transform for a time vector with a window length T_w and N_s samples. The time window T_w should be selected to be a whole number of fundamental cycles, and the time resolution $T_s=T_w/(N_s-1)$ should be set to achieve at least 100 samples per half carrier interval $\left(\text{i.e. } T_s<1/[200f_c]\right)$. Under these conditions the Fourier transform of (9) can be discretized as shown in (48) at the bottom of the page), where η and κ are both integers in the range $[0:N_s-1]$. Note that similar expressions can be developed for the regularly sampled cases. This result shows that the discrete Fourier transform of the multilevel PWM pulse train includes the discrete transform of the reference, and a summation of the discrete transforms for each of the sideband basis functions. Given that each sideband group has a narrow frequency range, this means that (48) can be used to accurately quantify the discrete PWM spectra for a small range of *m*. For example, the spectral plots shown in Fig. 8 to Fig. 9 would only require $m=3$.

The discrete spectral characterisation approach has been tested by calculating spectra for three and five level centred space vector modulators using MATLAB, with results shown in Fig. 10 and Fig. 11. The upper trace of both figures show the sampled space vector reference, and the phase voltage calculated from the sideband basis functions for $m=3$. The middle traces show the line to line voltage spectra, which are in precise agreement with the experimentally measured spectra in Figs 12 and 15 of [17], which provides a high degree of confidence in the numerical calculation. Finally the lower traces show FFT spectral results for the simulated line to line voltage, which again validates the discrete one-dimensional Fourier transform given in (48).

VII. CONCLUSIONS

This paper has presented a spectral analysis strategy for multilevel switched waveforms based on a one-dimensional Fourier series. The proposed approach separates the multilevel waveform into a spectral image of the reference, and sideband basis functions which can be expanded using a one-dimensional Fourier series. This methodology naturally incorporates regular sampling as part of the basic formulation, and closed form analytic spectral results can be obtained by evaluating a one-dimensional Fourier integral. For more complex reference waveforms, such as those generated by space vector modulators, a numerical discrete Fourier transform is presented that can accurately quantify the PWM spectrum for a specified number of sideband groups. All results are cross-referenced to previously published analytical results, and validated using numerically quantified spectral results calculated using MATLAB.

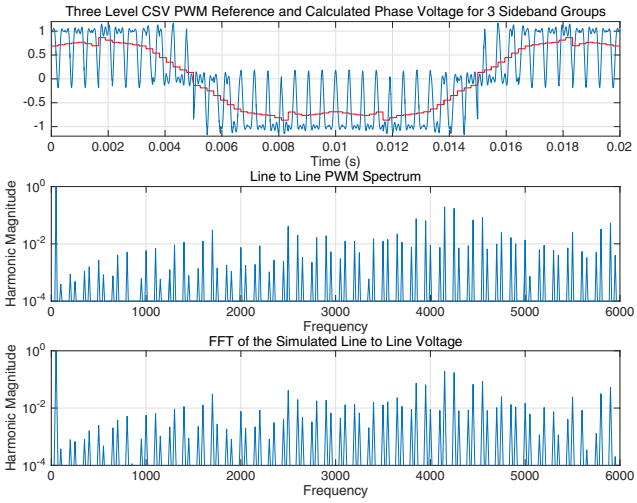

Fig. 10: Three level PD PWM with a centred space vector offset, *M=0.9, fo = 50Hz, fc = 2100Hz.*

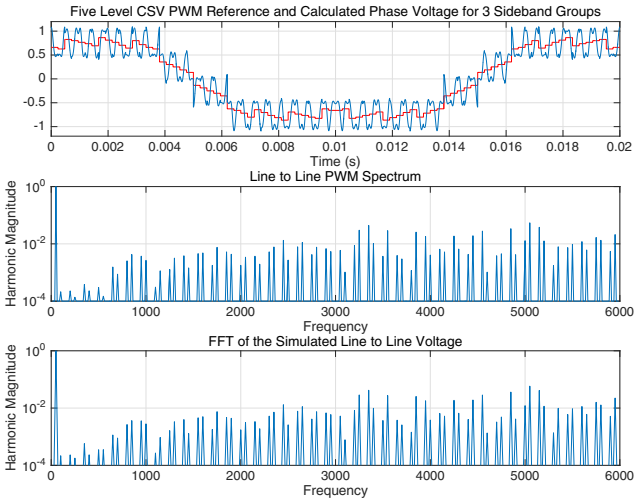

Fig. 11: Five level PD PWM with a centred space vector offset, *M=0.9, fo = 50Hz, fc = 2100Hz.*

ACKNOWLEDGEMENT

The authors acknowledge the financial support from the Australian Research Council under project DP140102437.

REFERENCES

[1] D. G. Holmes, T. A. Lipo, *Pulse width modulation for power converters – Principles and practice*, IEEE Press, 2003.

[2] J.G. Proakis and D.G. Manolakis, *Digital signal processing – Principles, algorithms and applications*, Prentice Hall, 3rd edn., 1996.

[3] H. Black, *Modulation Theory*, New York, USA: Van Nostrand, 1953.

[4] W. Bennet, "New results in the calculation of modulation products", *Bell Syst. Tech. J.*, vol. 12, pp. 228 – 243, Apr. 1933.

[5] M. Odavic, M. Sumner, P. Zanchetta and J. Clare, "A theoretical analysis of the harmonic content of PWM waveforms for multiple-frequency modulators", *IEEE Trans. Power Electron.*, vol. 25, no. 1, Jan. 2010, pp. 131 – 141.

[6] D.G. Holmes and B.P. McGrath, "Opportunities for harmonic cancellation with carrier-based pwm for two-level and multilevel cascaded inverters", *IEEE Trans. Ind. Applicat.*, vol. 37, no. 2, pp. 574 – 582, Mar./Apr. 2001.

[7] K. Ilves, L. Harnefors, S. Norrga and H.-P. Nee, "Analysis and operation of modular mulilevel converters with phase-shifted carrier pwm", *IEEE Trans. Power Electron.*, vol. 30, no. 1, pp. 268 – 283, Jan. 2015.

[8] B. Li, R. Yang, D. Xu, G. Wang, W. Wang and D. Xu, "Analysis of the phase-shifted carrier modulation for modular multilevel converters", *IEEE Trans. Power Electron.*, vol. 30, no. 1, pp. 297 – 310, Jan. 2015.

[9] R. Wilkinson, T. Meynard and H. du T. Mouton, "Natural balance of multicell converters : The general case", *IEEE Trans. Power Electron.*, vol. 21, no. 6, pp. 1658 – 1666, Nov. 2006.

[10] B.P. McGrath and D.G. Holmes, "Analytical modelling of voltage balance dynamics for a flying capacitor multilevel converter", *IEEE Trans. Power Electron.*, vol. 23, no. 2, pp. 543 – 550, Mar. 2008.

[11] W. van de Merwe, P. Hokayem and L. Stepanova, "Analysis of the N-cell single phase MMC natural balancing mechanism", *IEEE Jour. of Emerging and Selected Topics in Power Electron.*, vol. 2, no. 4, pp. 1149 – 1158, Dec. 2014.

[12] C.M. Wolf, M.W. Degner and F. Briz, "Analysis of current sampling errors in pwm, vsi drives", in Proc. IEEE Energy Conversion Congress and Exposition (ECCE), Denver USA, pp. 1770 – 1777, 2013.

[13] G. Carrara, S. Gardella, M. Marchesoni, R. Salutari and G. Sciutto, "A new multilevel pwm method: A theoretical analysis", *IEEE Trans Power Electron.*, vol. 7, no. 3, pp.497-505, Jul. 1992.

[14] B.P. McGrath and D.G. Holmes, "An analytical technique for the determination of spectral components of multilevel carrier-based pwm methods", *IEEE Trans. Ind. Electron.*, vol. 49, no. 4, pp. 847 – 857, 2002.

[15] B.P. McGrath and D.G. Holmes, "Multicarrier pwm strategies for multilevel inverters",*IEEE Trans. Ind. Electron.*, vol. 49, no. 4, pp. 858 – 867, 2002.

[16] W.H. Lau, B. Zhou and H.S.H. Chung, "Compact analytical solutions for determing the spectral characteristics of multicarrier-based multilevel pwm", *IEEE Trans. Circ. and Sys. I: Reg. Papers*, vol. 51, no. 8, Aug. 2004, pp. 1577 – 1585.

[17] B.P. McGrath and D.G. Holmes, "Optimized space vector switching sequences for multilevel inverters", *IEEE Trans. Power Electron.*, vol. 18, no. 6, pp. 1293 – 1301, Nov. 2003.

[18] H. du T. Mouton, B. P. McGrath, D. G. Holmes and R. H. Wilkinson, "One-dimensional spectral analysis of complex pwm waveforms using superposition", *IEEE Trans. Power Electron.*, vol. 29, no. 12, pp. 6762 – 6778, Dec. 2014.